Supporting Information

Correlated Structural-Optical Study of Single Nanocrystals in a Gap-bar Antenna: Effects of Plasmons on Excitonic Recombination Pathways

Feng Wang, Niladri S. Karan, Hue Minh Nguyen, Yagnaseni Ghosh, Chris J. Sheehan, Jennifer A. Hollingsworth and Han Htoon*

Center for Integrated Nanotechnologies, Materials Physics & Applications Division, Los Alamos National Laboratory, Los Alamos, New Mexico, 87545

Email: htoon@lanl.gov

Supplementary information:

S1. Synthesis of CdSe/CdS/SiO$_2$ core/shell/shell giant nanocrystal quantum dots (g-NQDs).

S2. Fabrication of g-NQDs-nanoantennas for correlated structural-optical study.

S3. Scattering spectrum of nanoantennas and emission/absorption spectra of g-NQDs.

S4. Additional PL traces of reference g-NQDs and g-NQDs-antennas coupled structures.

S5. Reduced metal quenching of single exciton.

S6. Average g-NQD exciton occupancy $\langle N \rangle \ll 1$.

S7. "Statistical" scalings of multiexciton states.

S8. Numerical simulation.

S1. Synthesis of CdSe/CdS/SiO₂ core/shell/shell giant nanocrystal quantum dots (g-NQDs).
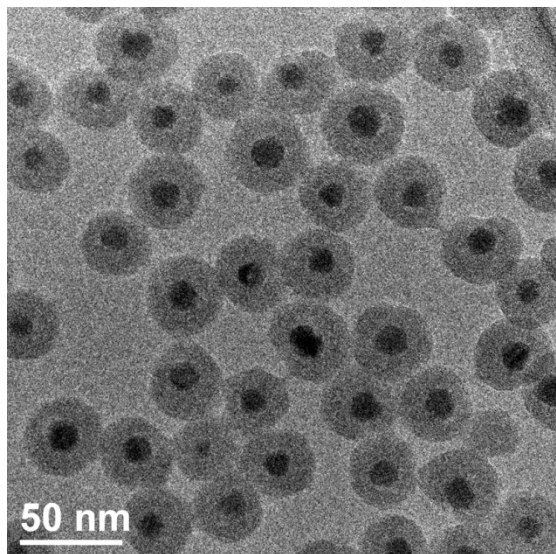
Figure S1. TEM image of the synthesized CdSe/CdS/SiO$_2$ core/shell/shell g-NQDs.

Materials:

Cadmium oxide (CdO, 99.95%), oleic acid (90%), 1-octadecene (ODE, 90%), 1-octadecane (OD, 90%) oleylamine (tech grade), sulfur powder (99.98%), selenium pellet (≥99.999%), and trioctyl phosphine (TOP) (97%) were purchased from Aldrich and used without further purification. Trioctyl phosphine oxide (TOPO) (90%) was purchased from Strem and used without further purification. Tetraethyl orthosilicate (TEOS, 99.999%), Igepal CO-520, NH$_4$OH solution (ACS reagent, 28-30%), (3-Aminopropyl)triethoxysilane (APTES, ≥ 98%) were purchased from Sigma-Aldrich. Cyclohexane (spectroscopy grade) was purchased from Acros Organics. Ethyl alcohol (ACS reagent, 94-96%) was purchased from Alfa-Aesar.

Synthesis:

In order to synthesize CdSe/CdS core (4 nm)/thick shell (16 monolayer) g-NQDs, a modified Successive Ionic Layer Adsorption and Reaction (SILAR) approach with a higher shell-growth temperature was adopted.[1] After obtaining the CdSe/16CdS core/shell NQDs, a reverse microemulsion method was used to perform the silica coating of the hydrophobic g-NQDs. [2, 3] Briefly, 0.5 ml Igepal CO-520 was added to 8 ml of cyclohexane and stirred for 15 mins in a 20 ml vial. Then, 450-µL g-NQD cyclohexane solution (optical density of CdSe 1S peak ~0.15) was added and stirred for another 15 min. 100 µL of NH$_4$OH and 80 µl of TEOS were then added to the mixture. The mixture was then stirred for 48 h at room temperature. The resulting g-

NQD/SiO$_2$ nanoparticles were precipitated using ethanol and collected by centrifugation at 10,000 rpm for 10 minutes. The product was redispersed in 10-ml nanopure water (18MΩ) with a final concentration of ~5 nM. For the APTES surface functionalization, 300 µl of APTES was added to the mixture and stirred for 12 h. Excess APTES was removed through centrifugation and washing. Finally, the APTES functionalized silica coated g-NQD were redispersed in (1:2) water:ethanol mixture.

S2. Fabrication of g-NQDs-nanoantennas for correlated structural-optical study.
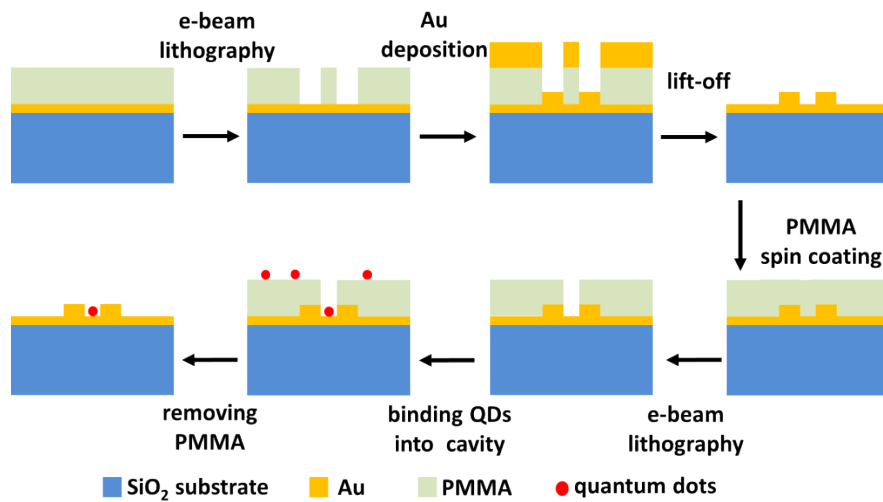
Figure S2. Schematic illustration of the fabrication of g-NQDs-nanoantenna coupled structures.

In order to precisely position the G-NQDs at the specific areas of the gap-bar nanocavities, two-step e-beam lithography was performed. At the beginning, cleaned glass substrate with 24 nm Au film deposited on top of it was prepared. The substrate was then spin-coated with 950 PMMA A4 (from MicroChem Corporation) at spin speed of 4500 rpm for 45s, achieving an approximately 190 nm PMMA film after baking. Then, the first step e-beam lithography and a 30s oxygen plasma etching were applied to define the lateral dimensions of the gap bar nano-antenna. The subsequent sputter deposition of 45 nm Au and lift-off process were accomplished to form the antennas. The second step lithography was employed to write circular holes on the positions where the quantum dots are required to be linked to. Our e-beam lithography system allows place the holes with ± 50 nm precision. After the second lithography, the sample was immersed into the diluted solution of APTES functionalized silica coated g-NQDs for 3 hours.

Next, the sample was rinsed with acetone for 1 minute and ethanol for another 1 minute and then blown dry with nitrogen gas.
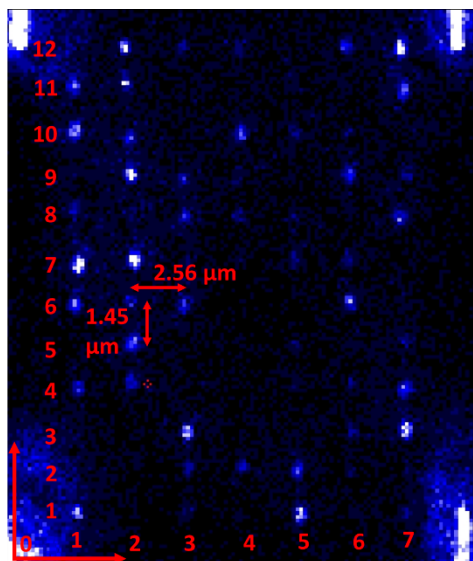
Figure S3. Confocal laser scanning image of the PL from one sub-array of the fabricated g-NQDs-nanoantennas.

In order to correlate the characterized emission spots in the optical measurements with their exact SEM pictures, a coordinate frame is necessary for the recognition of each individual structure. In brief, we fabricated a 100 × 100 μm antenna array, which consists of 5 × 5 sub-arrays with specific coordinates to locate them. In each sub-array, 12 × 7 g-NQDs-nanoantennas were fabricated with x-periodicity 2.56 μm and y-periodicity 1.45 μm. These periodicities were selected so that individual g-NQDs-nanoantennas structures can be excited by 300–500 nm diameter laser spot.

S3. Scattering spectrum of nanoantennas and emission/absorption spectra of g-NQDs.
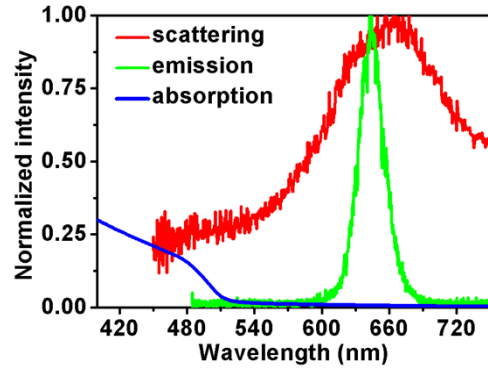
Figure S4. Measured scattering spectrum (red) of the fabricated gap-bar nanoantennas. Emission (green) and absorption (blue) spectra of the studied CdSe/CdS/SiO$_2$ g-NQDs. The peak of the scattering spectrum of the antennas matches the peak of the emission spectrum of the g-NQDs so that g-NQDs emission enhancement can be induced by the antenna.

S4. Additional PL traces of reference g-NQDs and g-NQDs-antennas coupled structures.
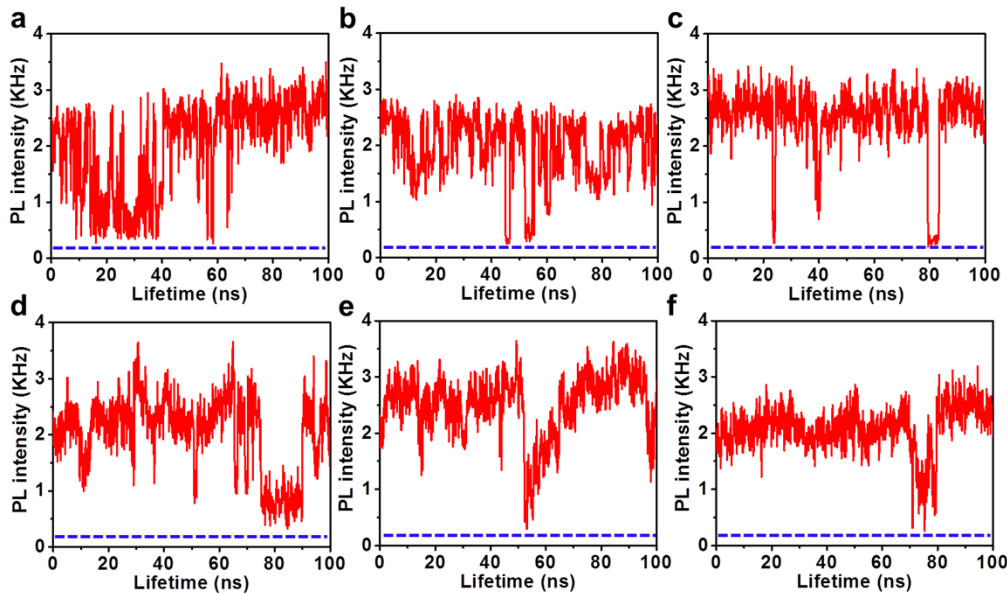

Figure S5. (a), (b) and (c) represent the measured PL blinking traces of the reference g-NQDs placed on glass substrate. (d), (e) and (f) represent the measured PL blinking traces of the g-NQDs placed in the gap-bar nanoantennas. Blue dotted line in each figure represents the background.

S5. Metal Induced Quenching of Single Exciton Emission.

Fig. 2a shows that g-NQDs coupled to antenna emit essentially at the same PL count rate as those spread on the glass substrate. Since this experiment was performed at low pump power where average exciton occupancy is less than 0.2, the PL is mainly contributed by the single exciton state. This result may suggest that metal induced PL quenching of single exciton has been suppressed so that the quenching losses become negligible. On the other hand, this result could also arise in a condition where metal induced PL quenching is compensated by the enhancement of laser excitation field by the antenna. However, both experimentally measured scattering spectrum (Fig. S4) and simulated local field intensity (Fig. 4a) clearly show that there is no plasmonic resonance and hence no field enhancement at the 405 nm laser excitation wavelength. In addition, the analysis on the pump intensity dependent PL saturation data (Fig.3a and 3b) gives identical absorption cross-sections for both g-NQDs placed on antennas and on glass substrates. This result further confirms that the enhancement of local excitation power is negligible. Based on this analysis, we conclude that the similar PL intensities between g-NQDs coupled to antenna and those on the glass could only be resulted from well-suppressed metal quenching.

S6. Contribution of higher order multi-exciton emission in g$^{(2)}$ experiment

A detail discussion on theory for g$^{(2)}$ experiment that provide a measure of Q_{2X}/Q_{1X} was given in ref. 5. Briefly, the area of the first side peak of the g$^{(2)}$ $g^{(2)}(T)$ is given by the probability of creation and emission of single exciton in two successive excitation event and can be expressed as $g^{(2)}(T) \approx (Q_{1x}\langle N \rangle)^2 + O(Q_{1x}Q_{2x}\langle N \rangle^3 + \cdots)$, where $\langle N \rangle$ represents the average g-NQD exciton occupancy per excitation pulse and $O(\langle N \rangle^3 + \cdots)$ represents terms with order of $\langle N \rangle^3$ and higher. The area of the center peak of the g$^{(2)}$ is expressed as $g^{(2)}(0) \approx Q_{1x}Q_{2x}\langle N \rangle^2 + O(Q_{1x}Q_{3x}\langle N \rangle^3 + \cdots)$. At low pump fluences when $\langle N \rangle \ll 1$ both terms scale with $\langle N \rangle^2$ and therefore the ratio $g^{(2)}(0)/g^{(2)}(T)$ approaches the value of Q_{2x}/Q_{1x}. Fig. 2(b) and 3(d) of ref. 5 has clearly shown that $g^{(2)}(0)/g^{(2)}(T)$ approach to a constant value reflecting Q_{2x}/Q_{1x} for $\langle N \rangle$ below 1 indicating that the contribution of higher order multi-exction state ($Q_{1x}Q_{3x}\langle N \rangle^3$ etc.) are negligible at this low pump fluence regime.
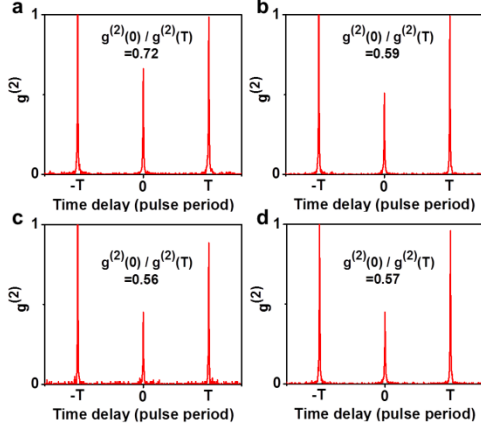
Figure S6. The measured g$^{(2)}$ curves of one representative g-NQD placed in gap-bar antenna under different excitation powers. (a) 0.072μW; (b) 0.036μW; (c) 0.012μW; (d) 0.008μW.

In this experiment, we first perform a similar pump dependent g$^{(2)}$ experiment to determine low pump regime. Fig. S6 shows the g$^{(2)}$ curves of a g-NQD in gap-bar antenna under four different excitation powers. Below 0.012μW pump power, we found $g^{(2)}(0)/g^{(2)}(T)$ remains stable with further decreasing the pump power to 0.008μW. We take 0.012μW as the optimum pump power for our experiment. We therefore believe that contribution from higher order multi-excitons in our current g$^{(2)}$ experiment is negligible. At 0.012μW excitation power, our measurement gives the count rates of the order of 2000 while background is only between 120–160 count. The g$^{(2)}$ trace we obtained therefore have very high signal to noise ratio as evidenced by the data. The contribution of the background on measured area ratio is therefore negligible.

S7. "Statistical" scalings of multiexciton states.

Q_{mX} is the quantum yield of m-exciton state and can be calculated from the ratio of radiative and non-radiative decay rates as:

$$Q_{mX} = 1/\left(1 + k_{nr}^{mX}/k_{r}^{mX}\right),$$

(S1)

where $k_{r/nr}^{mX}$ is the radiative/non-radiative recombination rates. Assuming that the Q_{1X} is equal to unity and then non-radiative decay channel is mainly due to Auger recombination, we can use "statistical" scalings to relate the radiative and Auger decay rates of multiexciton states ($k_{r/A}^{mX}$) to radiative decay rates of single exciton (k_r^X) and Auger rate of bi-exciton (k_A^{2X}) as:

$$k_r^{mX} = m^2 k_r^X \qquad \text{(S2a)}$$

$$k_A^{mX} = m^2 (m-1) k_A^{2X} / 4 \qquad \text{(S2b)}$$

Thus, we have:

$$Q_{2X} = \frac{1}{1 + k_A^{2X} / 4k_r^X} \qquad . \qquad \text{(S3)}$$

Based on eqn. S1-S4, we can express Q_{mX} in term of Q_{2X} as.

$$Q_{mX} = \frac{1}{1 + (m-1)(1 - Q_{2X}) / Q_{2X}} . \qquad \text{(S4)}$$

Equation S1, S2, S3 and S4 together with equation 1, 2 and 3 in the main manuscript allow us to model the PL saturation behavior of single g-NQDs in term of the bi-exciton quantum yields and the proportionality constant A that provide a direct measure of σ, absorption cross-section. Our prior study focused on bi-exciton quantum yields has validated this model.

S8. Numerical simulation.

To perform the numerical simulations, we used the CST-Microwave Studio software. The simulated gold bars antennas have bar length 900 nm, bar width 140 nm, thickness 45 nm and gap sizes 55 nm, which are in accordance with the real sample. The complex dielectric constant of Au for the simulation was obtained by fitting the data from Johnson and Christy,[4] while the refractive index of the SiO2 substrate was fixed at 1.45 for all wavelengths. For the calculation of excitation enhancement, a normal incident plane wave with 405 nm wavelength and periodic boundary conditions were used. For the calculation of emission enhancement, open boundary condition was used and dipoles were placed in the x-y plane, oriented 45 degrees to the long axis (y axis) of gap-bar antenna.

1 Y. Ghosh, B. D. Mangum, J. L. Casson, D. J. Williams, H. Htoon and J. A. Hollingsworth, *Journal of the American Chemical Society*, 2012, **134**, 9634-9643.
2 R. Koole, P. Liljeroth, C. d. M. Donega, D. Vanmaekelbergh and A. Meijerink, *Journal of the American Chemical Society*, 2006, **128**, 10436-10441.

3 D. K. Yi, S. T. Selvan, S. S. Lee, G. C. Papaefthymiou, D. Kundaliya and J. Y. Ying, *Journal of the American Chemical Society*, 2005, **127**, 4990-4991.

4 P. B. Johnson and R. W. Christy, *Physical Review B*, 1972, **6**, 4370-4379.

5 Y. -S. Park, A. V. Malko, J. Vela, Y. Chen, Y. Ghosh, F. Garcia-Santamaria, J. A. Hollingsworth, V. I. Klimov and H. Htoon, *Physical Review Letters*, 2011, **106**, 187401.